16th World Conference on Earthquake Engineering, 16WCEE 2017
Santiago Chile, January 9th to 13th 2017
Paper N° 2347
Registration Code: S- N1464747123

REAL-TIME HYBRID SIMULATION OF A RC STRUCTURE USING FORCE-BASED ELEMENTS AND ADVANCED INTEGRATION ALGORITHMS

C. Kolay[(1)], J.M. Ricles[(2)]

[(1)] Research Scientist I, ATLSS Engineering Research Center, Lehigh University, U.S.A., chk311@lehigh.edu
[(2)] Bruce G. Johnston Professor, Department of Civil and Environmental Engineering, Lehigh University, U.S.A., jmr5@lehigh.edu

Abstract

An accurate and efficient state determination of the analytical substructure plays an important role in real-time hybrid simulation (RTHS) of a structure subjected to seismic excitations. This becomes even more important for RTHS of reinforced concrete (RC) structures because the hysteretic behavior of RC members is complex and generally involve pinching, softening, and strength degradation in their force-deformation response. Such complex hysteretic behavior is better modeled using the force-based fiber element formulation compared with the stiffness-based approach. The main advantage of the force-based formulation, which stems from the enforcement of equilibrium along the element in a strict sense, is that the material nonlinearity can be modeled using a single element per structural member. This results in a significant reduction of the number of a model's degrees of freedom. However, the implementation of a force-based fiber element formulation in a standard stiffness-based finite element program requires an iterative state determination procedure to satisfy compatibility within a specified tolerance. This iterative procedure is not feasible for RTHS because convergence cannot be guaranteed in real time. This issue is addressed by implementing a force-based fiber element formulation with a fixed number of iterations for application to RTHS using an explicit direct integration algorithm. When the maximum number of iterations is reached, element end forces are corrected to re-establish compatibility and the unbalanced section forces are carried over to and corrected in the next integration time step. Using this implementation scheme and the modified KR-α (MKR-α) method, a recently developed family of unconditionally stable explicit parametrically dissipative direct integration algorithms, RTHS of a two-story RC special moment resisting frame (SMRF) building with a nonlinear viscous damper are performed under the maximum considered earthquake hazard level. The RC SMRF is modeled analytically using the force-based fiber element and the nonlinear viscous damper is modeled physically in the laboratory. The efficacy of the proposed iterative scheme is assessed based on RTHS results which show that an accurate solution can be obtained even when no iteration is performed at the element level.

Keywords: real-time hybrid simulation; force-based element; explicit dissipative algorithms; unconditional stability

1. Introduction

Real-time hybrid simulation (RTHS) is an efficient, economic, and viable alternative to more expensive shake table testing method for seismic simulation of civil infrastructure systems. In this simulation, seismic response of a structural system is simulated from coupled domains of *experimental (physical)* and *analytical (numerical) substructures*, where the former represents the part of the structure that cannot be modeled analytically/numerically with adequate accuracy and the latter constitutes the rest of the system. Dynamic response of the hybrid system is simulated by integrating the equations of motion generally using a direct integration algorithm. At each time step, the inertia, damping, and restoring forces for the analytical substructure are formulated analytically while these forces from the experimental substructure are measured physically. Compared with the conventional slow hybrid simulation (HS) method, the RTHS method involves many additional challenges including that the integration of the equations of motion for each time step needs to be performed in real time.

Numerous direct integration algorithms have been investigated in the past for application to RTHS. These algorithms can generally be classified as either *explicit* or *implicit*. An integration algorithm is said to be explicit if the solution at the current time step depends on the response(s) at the previous time step(s), otherwise it is implicit. Under nonlinear structural response implicit algorithms require an iterative solution procedure, whereas explicit algorithms do not require any iteration. Explicit algorithms are preferred for RTHS because an iterative

procedure is computationally intense and can introduce undesired hysteresis due to loading and unloading during iterations within the time step. However, explicit algorithms are generally only conditionally stable, which requires the time step size to be inversely proportional to the highest mode frequency present in the system. This imposes a severe restriction on the time step size, especially in the RTHS of structures with a large number of degrees of freedom (DOFs). To circumvent this, a new class of explicit algorithms that achieve unconditional stability through the use of *model-based* integration parameters was developed and applied to HS [1] and RTHS [2], [3]. In addition to unconditional stability, the need for controllable numerical dissipation to eliminate spurious participation of higher modes in an HS and RTHS was also realized. Kolay and Ricles [4] developed a one-parameter family of second-order accurate unconditionally stable explicit model-based algorithms with controllable numerical dissipation. Kolay et al. [5] applied this family of algorithms, referred to as the KR-α method, to a large-scale RTHS of a three-story steel frame building outfitted with nonlinear elastomeric dampers and demonstrated the efficacy of the controllable numerical dissipation in eliminating spurious participation of higher modes. The nondissipative algorithm of the KR-α method has an overshoot tendency for high-frequency modes, which is, however, reduced significantly with the introduction of numerical dissipation [6]. In order to further improve the overshoot characteristic and also enhance the stability behavior of the KR-α method when applied to nonlinear systems, a modified form of the method was developed [7]. In this study, this modified KR-α (MKR-α) method is applied to RTHS of a two-story reinforced concrete (RC) frame building outfitted with a nonlinear viscous damper, where the RC frame is modeled analytically and the damper is modeled physically in the laboratory.

Recent studies show that the force-based nonlinear beam-column fiber elements are better suited compared with the displacement-based formulation for modeling of complex hysteretic behavior of RC members which typically involves pinching, softening, and degradation in their force-deformation response. The main advantage of the force-based formulation stems from the use of force interpolation functions which enforce equilibrium along the element in a strict sense. This enables material nonlinearity to be modeled using a single element per structural member, and consequently, leads to a significant reduction in the number of structural model DOFs. This reduction is extremely beneficial in an RTHS because of the real-time computation demand of the simulation. However, implementation of the state determination of a nonlinear force-based element in a standard stiffness-based finite element program is not straight forward, and it requires an iterative procedure to satisfy the nonlinear section constitutive law and compatibility in terms of residual element deformations within a specified tolerance [8]. This type of iterative procedure is not feasible for RTHS application because convergence at the element level cannot be guaranteed in real time. Neuenhofer and Filippou [9] presented an alternative numerical implementation that bypasses the need for an iteration at the element level by accepting both residual element deformation, which violates compatibility at the element ends, and unbalanced section forces, which violates strict equilibrium along the element during each iteration at the structure level (e.g., Newton-Raphson). Upon convergence at the structure level, such violations are reduced to a specified numerical tolerance. However, this non-iterative implementation procedure is also not feasible for RTHS utilizing an explicit direct integration algorithm because no iteration is performed at the structure level. Therefore, a new implementation procedure is developed in this study for application to RTHS with an explicit direct integration algorithm. The key idea of the proposed implementation is to perform a fixed number of element iterations, correct the element end forces for residual element deformations to re-establish compatibility when the fixed number of iterations is reached, and carry over the unbalanced section forces to the next integration time step to correct for the equilibrium error.

The paper begins with a brief review of the formulation and numerical characteristics of the MKR-α method followed by the new implementation procedure for the state determination of a force-based element. RTHS of a two-story RC frame building outfitted with a nonlinear viscous damper and subjected to the maximum considered earthquake (MCE) hazard level [10] is then presented. Results are assessed to demonstrate the accuracy and efficiency of the proposed element implementation scheme.

2. Parametrically Dissipative Explicit Direct Integration Algorithms

In this section, the formulation and numerical characteristics of the MKR-α method [7] are briefly reviewed. Determination of the model-based integration parameters for application to RTHS are also discussed.

2.1. Formulation

In the MKR-α method the velocity $(\dot{\mathbf{X}}_{i+1})$ and displacement $(\mathbf{X}_{i+1})$ vectors at time t_{i+1} are calculated using the responses at time t_i (i.e., displacement $\mathbf{X}_i$, velocity $\dot{\mathbf{X}}_i$, and acceleration $\ddot{\mathbf{X}}_i$ vectors) as follows:

$$\dot{\boldsymbol{X}}_{i+1} = \dot{\boldsymbol{X}}_i + \Delta t \boldsymbol{\alpha_1} \ddot{\boldsymbol{X}}_i \tag{1}$$

$$\boldsymbol{X}_{i+1} = \boldsymbol{X}_i + \Delta t \dot{\boldsymbol{X}}_i + \Delta t^2 \boldsymbol{\alpha_2} \ddot{\boldsymbol{X}}_i \tag{2}$$

where $\boldsymbol{\alpha_1}$ and $\boldsymbol{\alpha_2}$ are the two model-based integration parameter matrices, which are determined as explained later, and Δt is the integration time step size. The controllable numerical dissipation is introduced in the method through weighing the inertia, damping, restoring, and excitation forces at the bounds of each time step except at the beginning $(t_0 = 0)$ where the conventional unweighted equations of motion are used as follows:

$$\boldsymbol{M} \hat{\ddot{\boldsymbol{X}}}_{i+1} + \boldsymbol{C} \dot{\boldsymbol{X}}_{i+1-\alpha_f} + \boldsymbol{R}_{i+1-\alpha_f} = \boldsymbol{F}_{i+1-\alpha_f} \tag{3}$$

$$\boldsymbol{M} \ddot{\boldsymbol{X}}_0 = \boldsymbol{F}_0 - \boldsymbol{C} \dot{\boldsymbol{X}}_0 - \boldsymbol{R}_0 \tag{4}$$

where $\mathbf{M}$ and $\mathbf{C}$ are the mass and damping matrices, respectively; $\mathbf{R}_{i+1}$ and $\mathbf{F}_{i+1}$ are the restoring and excitation force vectors, respectively. The time discrete combinations of acceleration, velocity, restoring force, and excitation force appearing in Eq. (3) are determined as follows:

$$\hat{\ddot{\boldsymbol{X}}}_{i+1} = (\boldsymbol{I} - \boldsymbol{\alpha_3}) \ddot{\boldsymbol{X}}_{i+1} + \boldsymbol{\alpha_3} \ddot{\boldsymbol{X}}_i \tag{5}$$

$$\dot{\boldsymbol{X}}_{i+1-\alpha_f} = (1 - \alpha_f) \dot{\boldsymbol{X}}_{i+1} + \alpha_f \dot{\boldsymbol{X}}_i \tag{6}$$

$$\boldsymbol{R}_{i+1-\alpha_f} = (1 - \alpha_f) \boldsymbol{R}_{i+1} + \alpha_f \boldsymbol{R}_i \tag{7}$$

$$\boldsymbol{F}_{i+1-\alpha_f} = (1 - \alpha_f) \boldsymbol{F}_{i+1} + \alpha_f \boldsymbol{F}_i \tag{8}$$

where $\boldsymbol{\alpha_3}$ is another model-based integration parameter matrix, and α_f is a scalar integration parameter. Using the eigenvalues of the amplification matrix of the generalized-α (G-α) method [11], the model-based integration parameters matrices were determined to be the following:

$$\boldsymbol{\alpha_1} = [\boldsymbol{M} + \gamma \Delta t \boldsymbol{C} + \beta \Delta t^2 \boldsymbol{K}]^{-1} \boldsymbol{M}$$

$$\boldsymbol{\alpha_2} = \left(\frac{1}{2} + \gamma\right) \boldsymbol{\alpha_1} \tag{9}$$

$$\boldsymbol{\alpha_3} = [\boldsymbol{M} + \gamma \Delta t \boldsymbol{C} + \beta \Delta t^2 \boldsymbol{K}]^{-1} [\alpha_m \boldsymbol{M} + \alpha_f \gamma \Delta t \boldsymbol{C} + \alpha_f \beta \Delta t^2 \boldsymbol{K}]$$

where $\mathbf{K}$ is the initial elastic stiffness matrix of the system. In order to achieve second-order accuracy, unconditional stability for linear systems, an improved overshoot characteristic, and an optimal combination of high-frequency and low-frequency numerical dissipation, the scalar integration parameters γ, β, α_m, and α_f were related to the user defined high-frequency spectral radius ρ_∞ as follows:

$$\gamma = \frac{1}{2} - \alpha_m + \alpha_f \qquad \beta = \frac{1}{2}\left(\gamma + \frac{1}{2}\right) \tag{10}$$

$$\alpha_m = \frac{2\rho_\infty^3 + \rho_\infty^2 - 1}{\rho_\infty^3 + \rho_\infty^2 + \rho_\infty + 1} \qquad \alpha_f = \frac{\rho_\infty}{\rho_\infty + 1} \tag{11}$$

where the free parameter ρ_∞ varies in the range of $0 \leq \rho_\infty \leq 1$. Thus, the MKR-$\alpha$ method is a family of algorithms having only one free user defined parameter ρ_∞. For $\rho_\infty = 1$, the MKR-α method becomes nondissipative. As ρ_∞ reduces numerical dissipation increases, and $\rho_\infty = 0$ produces asymptotic annihilation, i.e., 100% numerical dissipation in the high-frequency.

2.2. Numerical characteristics

Numerical dispersion and dissipation of an integration algorithm are generally measured in terms of relative period error (PE) and equivalent damping ratio $(\bar{\xi})$, respectively. In order to compare these numerical characteristics of the MKR-α method with the KR-α [4] and the implicit G-α [11] methods based on the same high-frequency dissipation a new parameter ρ_∞^* is introduced which is related to the parameter ρ_∞ as follows:

$$\rho_\infty^* = \rho_\infty \quad \text{for KR-}\alpha \text{ and G-}\alpha; \qquad \rho_\infty^* = \rho_\infty^2 \quad \text{for MKR-}\alpha \tag{12}$$

where $0 \leq \rho_\infty^* \leq 1$. Fig. 1 presents the PE and equivalent damping ratio $(\bar{\xi})$ for the MKR-α method compared with the KR-α and G-α methods, where T, $\bar{T}$, and ω are the undamped natural period, apparent period, and

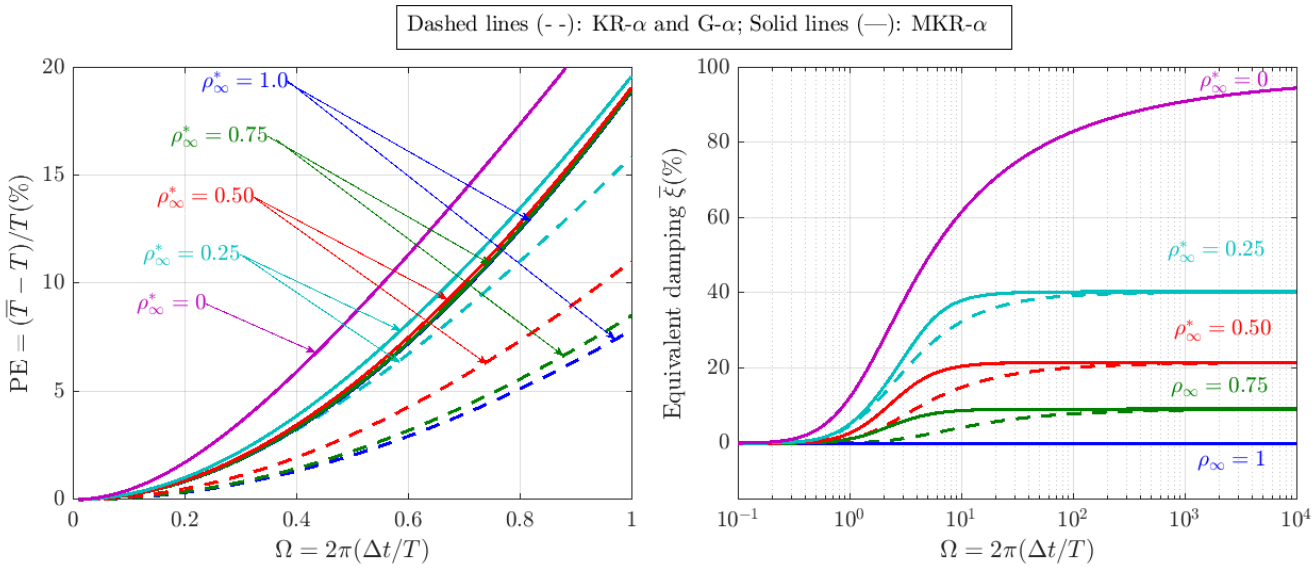

Fig. 1: Numerical dispersion and dissipation characteristics of the MKR-α method.

undamped natural frequency of an SDOF system, respectively; and $\Omega = \omega\Delta t$ is the dimensionless frequency. The figure shows that the MKR-α method is slightly more dispersive and dissipative compared with the KR-α and G-α methods for a given value of the same high-frequency dissipation, i.e., ρ_∞^*. Note that the numerical dispersion and dissipation characteristics of the KR-α and G-α methods are identical. The figure shows that the PE and $\bar{\xi}$ increase with increasing Ω and reducing values of ρ_∞^*. However, in the low-frequency regime, typically $\frac{\Delta t}{T} \leq \frac{1}{20}$ or $\Omega \leq 0.1\pi$, the PE and $\bar{\xi}$ are small for all of the methods indicating that the low-frequency mode response is negligibly influenced by numerical dissipation. On the other hand, adequate high-frequency numerical dissipation can be obtained to damp out any spurious participation of higher modes in an MDOF system. Furthermore, observe that the increase in the PE and $\bar{\xi}$ of the MKR-α method compared with the KR-α and G-α methods is small in the low-frequency regime. It should be pointed out that the aforesaid small increase in the PE and $\bar{\xi}$ for the MKR-α method in the low-frequency regime is the consequence of improving the overshoot characteristic and nonlinear stability behavior of the KR-α method by the MKR-α method [7]. Other numerical characteristics of the MKR-α method can be found in ref. [7].

2.3. Model-based integration parameters for real-time hybrid simulation

In an RTHS, the system matrices $\mathbf{M}$, $\mathbf{C}$, and $\mathbf{K}$ appearing in the model-based integration parameters in Eq. (9) must be determined based on the complete hybrid system. Therefore, these matrices, hereafter denoted with the subscript IP, can be formulated as follows:

$$\begin{aligned} \boldsymbol{M}_{IP} &= \boldsymbol{M} + \boldsymbol{M}^e \\ \boldsymbol{C}_{IP} &= \boldsymbol{C} + \boldsymbol{C}_{eq}^e \\ \boldsymbol{K}_{IP} &= \boldsymbol{K}_I^a + \boldsymbol{K}_{eq}^e \end{aligned} \tag{13}$$

where $\mathbf{M}$ is the analytically defined mass matrix of the complete hybrid system which excludes the mass of the experimental substructure $\mathbf{M}^e$; $\mathbf{C}$ is the inherent damping matrix of the complete hybrid system the effect of which is not accounted for in the analytically determined and/or experimentally measured restoring forces; $\mathbf{C}_{eq}^e$ is the equivalent damping matrix of the experimental substructures; $\mathbf{K}_I^a$ and $\mathbf{K}_{eq}^e$ are the initial elastic stiffness matrix of the analytical substructure and equivalent initial elastic stiffness matrix of the experimental substructure, respectively.

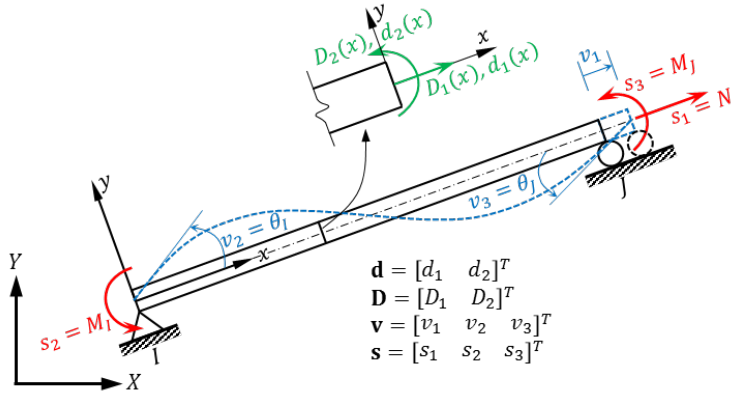

Fig. 2: Forces ($\mathbf{s}$, $\mathbf{D}(x)$) and deformations ($\mathbf{v}$, $\mathbf{d}(x)$) at the element and section level for a two dimensional frame element in simply supported basic system.

3. Force-Based Fiber Element Implementation

Fig. 2 shows a two dimensional force-based frame element in the simply supported basic system where $\mathbf{s}$ and $\mathbf{v}$ are the element end restoring forces and deformations, respectively; and $\mathbf{D}(x)$ and $\mathbf{d}(x)$ are the section forces and deformations, respectively. Based on the iterative state determination procedure of Spacone et al. [8] and the non-iterative implementation of Neuenhofer and Filippou [9], a new implementation scheme for the state determination of force-based frame elements is developed for application to RTHS using an explicit direct integration algorithm as presented in Fig. 3. The key idea of this new implementation scheme is to limit the number of iterations to a predefined maximum number of iterations $maxIter$ and carry the unbalanced section forces $\left(\mathbf{D}_U(x)\right)_i$ that result due to the limiting number of iterations from the ith integration time step to the next $(i+1)$th time step and include it in the current section force increment $\Delta\mathbf{D}^{j=1}(x)$ vector only for the first iteration $j = 1$ as shown in the sixth row of blocks in Fig. 3. The subsequent steps follow the iterative procedure of Spacone et al. [8] until the check for the maximum number of iterations ($j = maxIter$) which is the second last row in the figure. Once the maximum number of iterations is reached and if the element is not converged with a predefined tolerance, which is discussed below, the element end forces are corrected using the current element tangent stiffness matrix $(\mathbf{K})_{i+1}$ and the residual element deformations $\mathbf{v}_r^j$ in order to re-establish compatibility, and the unbalanced section forces $\left(\mathbf{D}_U(x)\right)_{i+1}$ at the current time step are calculated as shown in the figure. This unbalanced section forces are then carried to the next time step and added with the incremental section forces for the first iteration, as noted earlier. The influence of carrying over the unbalanced section forces and applying the aforesaid corrections were investigated through numerical simulation in ref. [7]. It was shown that the proposed implementation scheme with $maxIter = 1$, i.e., no iteration at the element level can also produce an adequately accurate solution.

The element convergence at the end of an iteration, except for the first iteration ($j = 1$), is checked using the energy based criteria proposed by Taucer et al. [12] as follows:

$$\frac{(\Delta \boldsymbol{s}^j)^T(\Delta \boldsymbol{v}^j)}{(\Delta \boldsymbol{s}^{j=1})^T(\Delta \boldsymbol{v}^{j=1})} = \frac{\left(\Delta \boldsymbol{v}_r^{j-1}\right)^T \boldsymbol{K}^{j-1}\left(\Delta \boldsymbol{v}_r^{j-1}\right)}{((\Delta \boldsymbol{v})_{i+1})^T(\boldsymbol{K})_i(\Delta \boldsymbol{v})_{i+1}} \leq Etol \qquad \text{for } j > 1 \tag{14}$$

Typically, a default value of $Etol = 10^{-16}$ is assigned [12].

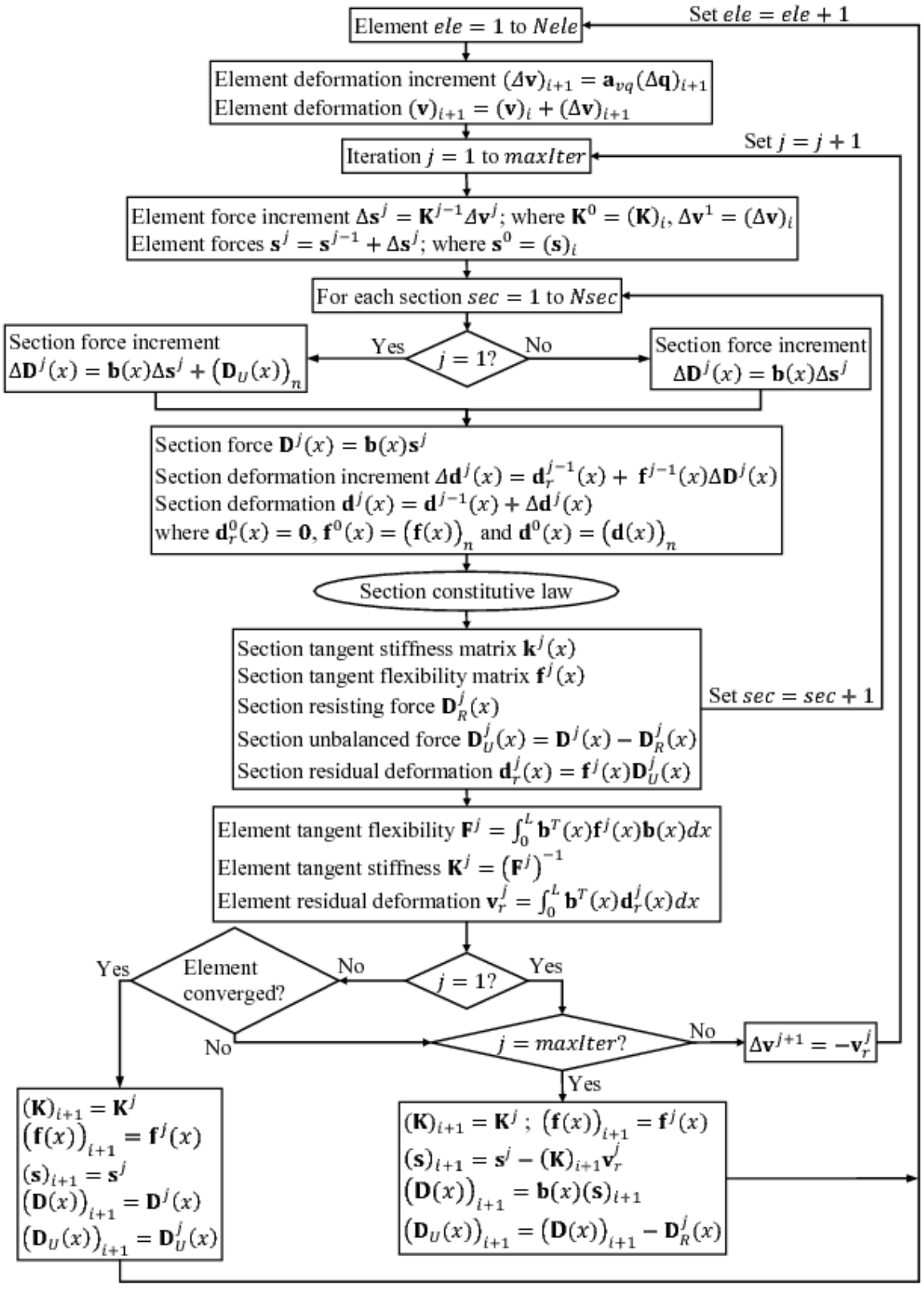

Fig. 3: State determination of force-based frame element at time step $(i + 1)$ in RTHS using an explicit direct integration algorithm.

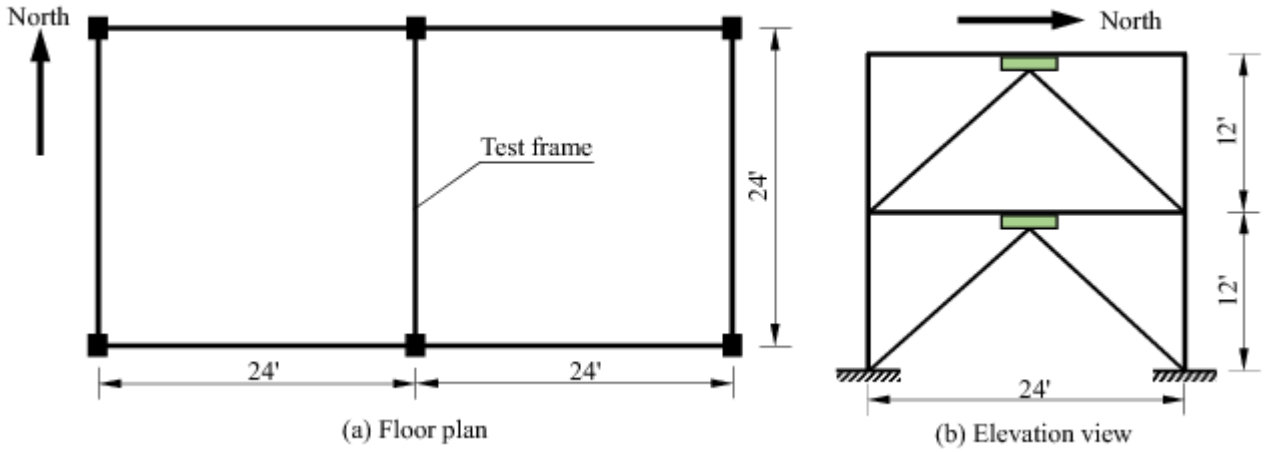

Fig. 4: Two-story reinforced concrete prototype building with nonlinear viscous dampers.

4. Real-Time Hybrid Simulation Configuration

In order to assess the efficacy of the proposed element implement scheme in RTHS, a simple two-story RC prototype building shown in Fig. 4 was considered. The building has two and three special moment resisting frames (SMRFs) in the east-west and north-south directions, respectively. The building is assumed to be a retail store located in the Los Angeles area on a stiff soil site. Thus, a design spectrum [10] with parameters $S_{DS} = 1.0$, $S_{D1} = 0.6$, $T_0 = 0.12$ s, and $T_S = 0.6$ s represents the design basis earthquake (DBE) hazard level. The RC SMRFs without the dampers were designed for strength requirements as per ASCE 7 [10]. The approximate design period of the building was determined to be $T_a = 0.39$ s [10]. Seismic loads on the prototype building were determined using the equivalent lateral force procedure, where the seismic response coefficient was determined to be $C_s = 0.125$ [10]. For determining the member design forces the appropriate load combinations according to ASCE 7 [10] were considered. The RC beam column members of the SMRFs were designed and detailed according to ACI 318 [13]. In order to perform an RTHS, nonlinear viscous dampers were added to the north-south SMRF located at the middle of the floor plan as shown in Fig. 4(b). The braces of the prototype test frame were designed to remain elastic for the maximum damper force capacity and be stiff enough to make the damper effective [7].

For conducting RTHS only one nonlinear viscous damper was available. Preliminary numerical analysis of the prototype test frame indicated that the story drift under the DBE and MCE level earthquakes are larger in the second story. Therefore, the nonlinear viscous damper was added to the second story. The RC SMRF, the braces, and the associated seismic masses were modeled analytically and the nonlinear viscous damper was modeled physically in the laboratory as shown in Fig. 5.

4.1. Analytical substructure

An FE model of the analytical substructure was developed in HybridFEM [14], a MATLAB and Simulink based software for conducting nonlinear dynamic analysis and RTHS. The RC SMRF was modeled using the force-based fiber elements as shown in Fig. 5(a). Each story column was modeled using one force-based element, while each beam was modeled using two force-based elements. Each beam was divided into two elements to collect the inertia forces at the middle of the beam using a rigid floor diaphragm as shown in the figure. The floor masses were lumped on a lean-on column as shown in the figure which accounts for the P-Δ effects. The beam-column joints were assumed to be rigid and modeled using stiff linear elastic elements. Each brace was modeled using a linear elastic beam-column element with moment release at the ends of the element.

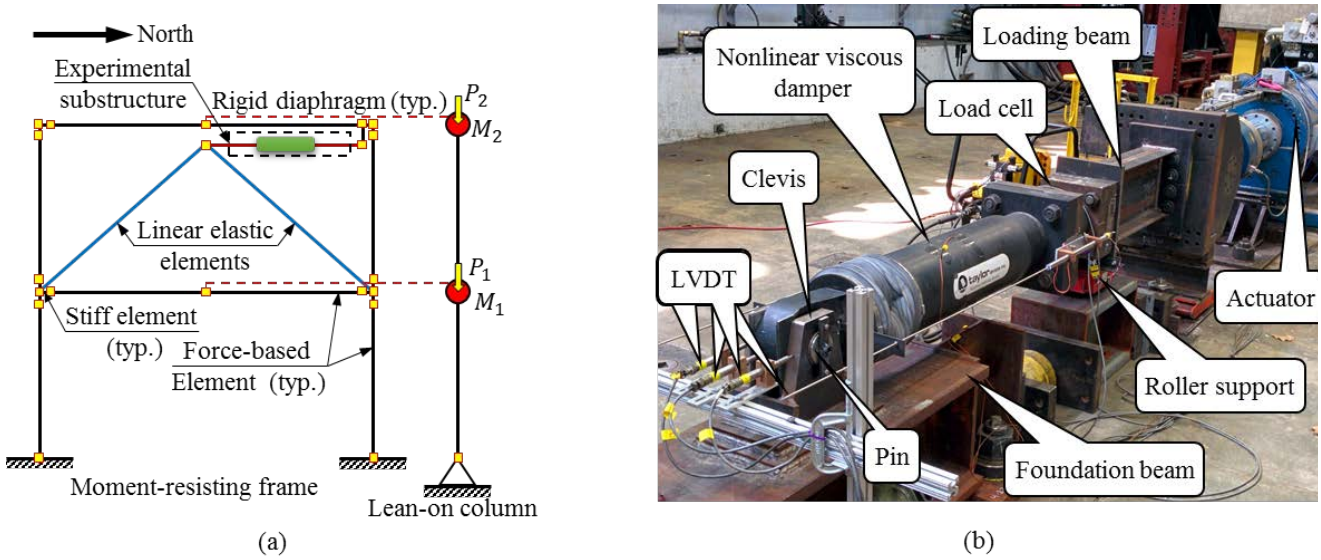

Fig. 5: RTHS configuration (a) FE model of the analytical substructure, and (b) test setup of the experimental substructure.

For strain-softening type section behavior commonly observed in RC members with high axial loads, force-based elements are known to have strain localization issues [15]. This leads to loss of objectivity meaning that the element and section responses are sensitive to the number of integration points (sections) considered along the element. Numerous studies have been conducted to regularize the force-based element response with strain-softening section behavior. In this study, the plastic hinge integration method of Scott and Fenves [16] was adopted for the force-based elements in order to obtain objective element and section responses. The key idea of this element integration scheme is to assign physically meaningful weights based on the plastic hinge length to the element end integration points where strains localize. The plastic hinge lengths for beams and column members of the prototype RC SMRF, required in the element integration scheme, were calculated using the equation proposed by Paulay and Priestley [17].

The section constitutive law for each integration point was modeled using the fiber section. Along the depth, the core and cover parts of a RC member section were divided into 5 and 10 fibers which resulted in a total of 20 concrete fibers at each section. The steel reinforcement bars were modeled using steel fibers. The concrete fiber constitutive law was modeled using the modified Kent-Park model [18] with degraded linear unloading and reloading paths according to the work of Karsan and Jirsa [19]. No tensile strength was considered in the model. Steel reinforcement material was modeled using a modified Giuffre-Menegotto-Pinto model [20], [21] with isotropic strain hardening.

Inherent damping in the analytical substructure was modeled using a combination of mass, initial stiffness, and tangent stiffness proportional damping models, where the tangent stiffness matrix was used for the force-based elements and initial stiffness matrix was used for all other elements. To enable efficient computation of the damping forces at each time step, the tangent stiffness proportional damping forces for the force-based elements were determined within the state determination procedure of the force-based elements. These damping forces were then appropriately added with the mass and initial stiffness proportional damping forces for the analytical substructure excluding the force-based elements, where the mass and initial stiffness proportional damping matrix was formed at the beginning of the simulation.

4.2. Experimental substructure

Fig. 5(b) shows the test setup for the experimental substructure consisting of a nonlinear viscous damper. The damper was manufactured by Taylor Device Inc. and has a nominal force capacity of 600 kN and a maximum

stroke of ± 125 mm. As shown in the figure, the damper was loaded by a hydraulic actuator. The actuator (capacity 1700 kN) was outfitted with 3 servo-valves to enable a maximum velocity of 1140 mm/s to be achieved when it is free-standing (zero force). During the RTHS, the damper force was measured using a load cell located between the damper end plate and the loading beam. The damper deformation could be measured using the LVDTs mounted between the damper end plate on one end and the damper piston at the other end. Damper deformation measured in this way will exclude any elastic flexibility of the test setup that arise from the elastic flexibility of the clevis, foundation beam, loading beam, actuator reaction frame and various connections. For the sake of simplicity, the connections between the braces and damper, and the damper and RC SMRF roof beam were not modeled analytically. To account for these flexibilities it was decided to include some flexibility of the test setup in measuring the damper deformation. Therefore, instead of using the damper deformation from the mounted LVDTs, the actuator displacement measured using the temposonic position sensor built into the actuator was considered as the damper deformation.

As noted earlier, in Eq. (13) the mass matrix $\mathbf{M}^e$, equivalent damping matrix $\mathbf{C}_{eq}^e$, and equivalent initial stiffness matrix $\mathbf{K}_{eq}^e$ of the experimental substructure are required for determination of the model-based integration parameters of the MKR-α method. In this study, $\mathbf{M}^e$ was neglected considering the mass of the damper to be negligible compared with the analytically modeled mass matrix $\mathbf{M}$. In order to determine $\mathbf{C}_{eq}^e$and $\mathbf{K}_{eq}^e$, a nonlinear Maxwell damper model with a linear spring and nonlinear dashpot in series was developed and the model parameters were identified based on damper characterization tests. The nonlinear Maxwell damper model was then linearized at a small threshold velocity and an equivalent Kelvin-Voigt model (a linear spring and a linear dashpot in parallel) of the linearized Maxwell damper model was developed which led to the determination of $\mathbf{C}_{eq}^e$ and $\mathbf{K}_{eq}^e$. It should be pointed out that $\mathbf{C}_{eq}^e$ and $\mathbf{K}_{eq}^e$ are functions of the excitation frequency due to the frequency dependent behavior of the Maxwell model, which is generally used to model the frequency-dependent response of nonlinear viscous dampers. Thus, the model-based integration parameters (see Eqs. (9) and (13)) become frequency dependent. The influence of this frequency dependency on the stability and accuracy of RTHS was thoroughly investigated in ref. [7]. It was shown that numerical dissipation provided by the MKR-α method plays an important role in performing stable RTHS when $\mathbf{C}_{eq}^e$and $\mathbf{K}_{eq}^e$ values are underestimated, which is associated with the frequency dependent estimation of these matrices. It was also found that the accuracy of RTHS results is not sensitive to this frequency dependency provided that stability is achieved.

5. Real-Time Hybrid Simulation Results

A series of RTHS were conducted using the 1999 Chi-Chi earthquake record scaled to the MCE hazard level. For numerical dissipation, $\rho_\infty^* = 0.75$ was used in the MKR-α method. An integration time step size $\Delta t = \frac{3}{1024}$ s was used, which is the smallest time step size that can be used to complete the numerical computation at each time step in real time with a maximum of two iterations ($maxIter = 2$) for each force-based elements in the analytical substructure. Through numerical simulation of the analytical substructure it was found that $maxIter = 2$ produces an accurate solution [7]. Even for the case of $maxIter = 1$ an adequately accurate solution is achieved in the numerical simulation of the analytical substructure when the equilibrium and compatibility corrections are made as discussed earlier. On the other hand, when the unbalanced section forces and the residual element deformations are neglected, $maxIter = 1$ produces a large error in the solution [7]. Therefore, in RTHS the unbalanced section forces were carried over to the next time step and the aforesaid corrections were made, and the tests were conducted using $maxIter = 1$ and 2. It should be pointed out that both $maxIter = 1$ and 2 require a minimum time step size of $\Delta t = \frac{3}{1024}$ s because of the other real-time computations that are involved in the direct integration of the equations of motion (see ref. [7] for more details).

In order to demonstrate that the fixed number of iteration scheme provides an accurate solution in an RTHS, numerical simulation (offline simulation) of each RTHS was performed using the measured damper force and allowing all the force-based elements to converge with $Etol = 10^{-16}$. It should be noted that a maximum of about 8 iterations are required for all the elements to converge with this tolerance. Fig. 6 presents a comparison

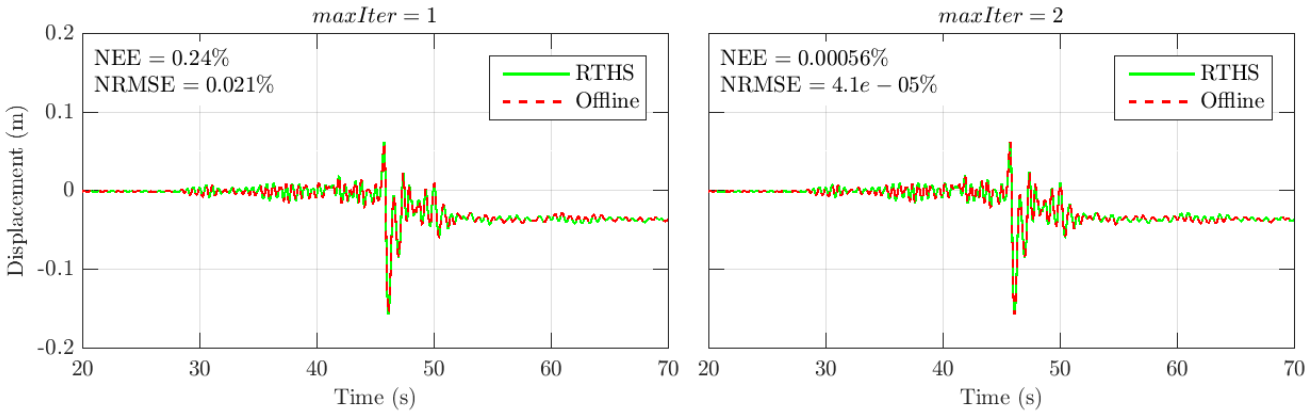

Fig. 6: Comparison of roof displacement time history from RTHS and offline simulation using the measured damper force and allowing the force-based elements to converge with $Etol = 10^{-16}$.

of the roof displacement time history from RTHS with the offline simulation for $maxIter = 1$ and 2. The normalized energy error (NEE) and normalized root mean square error (NRMSE) are calculated using Eq. (15), and are also noted in the figure.

$$\text{NEE} = \left|\frac{\sum_{n=1}^{N}(x_n)^2 - \sum_{n=1}^{N}(\hat{x}_n)^2}{\sum_{n=1}^{N}(\hat{x}_n)^2}\right| \qquad \text{NRMSE} = \frac{\sqrt{\frac{1}{N}\sum_{n=1}^{N}(x_n - \hat{x}_n)^2}}{max(\hat{\boldsymbol{x}}) - min(\hat{\boldsymbol{x}})} \tag{15}$$

Table 1: Comparison of story drift (%) for two different values of maximum number of element level iterations.

Story	$maxIter = 1$	$maxIter = 2$
1	3.35	3.39
2	1.03	1.01

where x and $\hat{x}$ are the responses from offline simulation and RTHS, respectively. Fig. 6 indicates that $maxIter = 1$ provides an adequately accurate solution and the accuracy increases further when $maxIter$ is increased to 2. This results indicate that had all the force-based elements been allowed to converge in real time with the default value of $Etol = 10^{-16}$ by some hypothetical means (e.g., very high end computational capabilities) the RTHS results would been practically the same as that obtained using $maxIter = 1$ or 2. In order to compare the RTHS results for the two values of $maxIter$, Fig. 7 presents the moment-curvature section response at the first-story south side column base and the measured hysteretic damper response. The results indicate negligible difference between the two RTHS. The comparison of the story drifts from the two RTHS presented in Table 1 also indicates a negligible difference between $maxIter = 1$ and 2. These, results further demonstrate that $maxIter = 1$ also produces an accurate result. It should be pointed out that the displacement time history in Fig. 6, moment-curvature section response in Fig. 7(a), and the story-drifts in Table 1 are all indicative of the significant nonlinear inelastic deformations that occur in the RC SMRF. Nevertheless, the proposed fixed number of iterations scheme is efficient and accurate even when no iteration is performed.

6. Summary and Conclusions

The formulation of the second-order accurate unconditionally stabile explicit parametrically dissipative MKR-α method which features improved overshoot characteristic and enhanced nonlinear stability was briefly reviewed. Numerical dispersion and dissipation characteristics of the method were compared with the KR-α and G-α methods. The comparison indicates that the MKR-α method is slightly more dispersive and dissipative in the low-frequency regime for a given level of high-frequency dissipation. Nevertheless, the low-frequency modes in an MDOF system is negligibly influenced by the numerical dissipation provided by the method. It should be

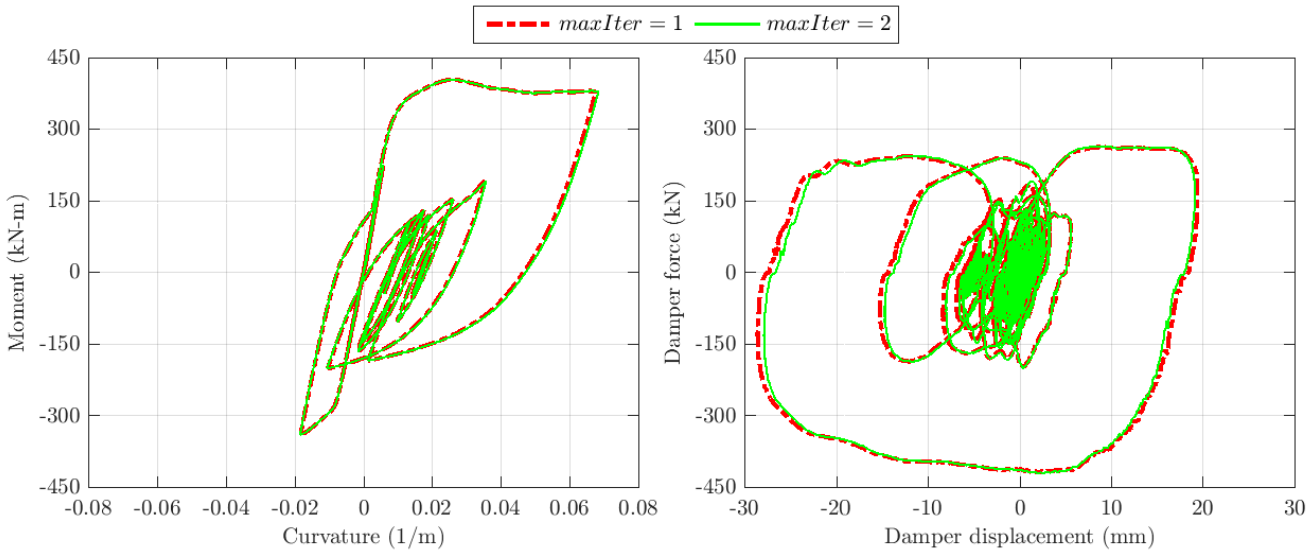

Fig. 7: Comparison of RTHS results for two different values of $maxIter$: (a) moment-curvature section response at the column base, south side, and (b) damper response.

noted that although the MKR-α method features an improved stability characteristic for nonlinear systems it can pose a stability problem for stiffening type of response like any other model-based algorithm. Nevertheless, this limitation can be addressed by identifying or determining the model-based parameters corresponding to the stiffest state of the system.

Using the MKR-α method RTHS of a two-story RC frame building outfitted with a nonlinear viscous damper in the second-story was conducted. The RC SMRF, braces, and seismic masses were modeled analytically and the nonlinear viscous damper was modeled physically in the laboratory. In order to better model the complex hysteretic behavior of RC members, nonlinear force-based fiber elements were used. A new implementation scheme for the state determination of force-based elements for application to RTHS using an explicit direct integration algorithm was developed based on a fixed number of element level iterations. Because of the fixed number of iterations, unbalanced section forces, which violate equilibrium, and residual element deformations, which violate compatibility, exist at each time step. In order to re-establish compatibility, the element end forces are corrected using the residual element deformations and the current tangent stiffness matrix. The unbalanced section forces are carried to the next integration time step and corrected. The RTHS results indicate that the proposed implementation scheme is efficient and accurate and can also be adopted for large-scale numerical simulation application.

7. Acknowledgements

The authors acknowledge the financial support provided by the P.C. Rossin College of Engineering and Applied Science (RCEAS) fellowship and the Gibson fellowship awarded to the first author through the Department of Civil and Environmental Engineering, Lehigh University. The testing was performed at the NHERI Lehigh Experimental Facility, whose operation is supported by the National Science Foundation.

8. References

[1] S.-Y. Chang, "Explicit pseudodynamic algorithm with unconditional stability," *J. Eng. Mech.*, vol. 128, no. 9, pp. 935–947, 2002.

[2] C. Chen and J. M. Ricles, "Development of direct integration algorithms for structural dynamics using discrete control theory," *J. Eng. Mech.*, vol. 134, no. 8, pp. 676–683, 2008.

[3] C. Chen, J. M. Ricles, T. M. Marullo, and O. Mercan, "Real-time hybrid testing using the unconditionally stable explicit CR integration algorithm," *Earthq. Eng. Struct. Dyn.*, vol. 38, no. 1, pp. 23–44, 2009.

[4] C. Kolay and J. M. Ricles, "Development of a family of unconditionally stable explicit direct integration algorithms with controllable numerical energy dissipation," *Earthq. Eng. Struct. Dyn.*, vol. 43, no. 9, pp. 1361–1380, 2014.

[5] C. Kolay, J. M. Ricles, T. M. Marullo, A. Mahvashmohammadi, and R. Sause, "Implementation and application of the unconditionally stable explicit parametrically dissipative KR-α method for real-time hybrid simulation," *Earthq. Eng. Struct. Dyn.*, vol. 44, no. 5, pp. 735–755, 2015.

[6] C. Kolay and J. M. Ricles, "Assessment of explicit and semi-explicit classes of model-based algorithms for direct integration in structural dynamics," *Int. J. Numer. Methods Eng.*, vol. 107, no. 1, pp. 49–73, 2016.

[7] C. Kolay, "Parametrically Dissipative Explicit Direct Integration Algorithms for Computational and Experimental Structural Dynamics," PhD Dissertation, Dept. of Civil and Env. Engg., Lehigh University, 2016.

[8] E. Spacone, V. Ciampi, and F. C. Filippou, "Mixed formulation of nonlinear beam finite element," *Comput. Struct.*, vol. 58, no. I, pp. 71–83, 1996.

[9] A. Neuenhofer and F. C. Filippou, "Evaluation of nonlinear frame finite-element models," *J. Struct. Eng.*, vol. 123, no. 7, pp. 958–966, 1997.

[10] ASCE, *Minimum Design Loads for Buildings and Other Structures (ASCE/SEI 7-10)*. Reston, Virginia, U.S.A.: American Society of Civil Engineers, 2010.

[11] J. Chung and G. M. Hulbert, "A time integration algorithm for structural dynamics with improved numerical dissipation: the generalized-α method," *J. Appl. Mech.*, vol. 60, no. 2, pp. 371–375, 1993.

[12] F. F. Taucer, E. Spacone, and F. C. Filippou, "A fiber beam-column element for seismic response analysis of reinforced concrete structures," 1991.

[13] ACI, *Building Code Requirements for Structural Concrete and Commentary (ACI 318-11)*. Farmington Hills, MI, U.S.A.: American Concrete Institute, 2011.

[14] T. L. Karavasilis, C.-Y. Seo, and J. M. Ricles, "HybridFEM: A program for dynamic time history analysis and real-time hybrid simulation," Bethlehem, PA, ATLSS Report, 2012.

[15] J. Coleman and E. Spacone, "Localization issues in force-based frame elements," *J. Struct. Eng.*, vol. 127, no. 11, pp. 1257–1265, 2001.

[16] M. H. Scott and G. L. Fenves, "Plastic hinge integration methods for force-based beam–column elements," *J. Struct. Eng.*, vol. 132, no. 2, pp. 244–252, 2006.

[17] T. Paulay and M. Priestley, *Seismic Design of Reinforced Concrete and Masonry Buildings*, 1st ed. New York: John Wiley & Sons, Inc., 1992.

[18] B. D. Scott, R. Park, and M. J. N. Priestley, "Stress-strain behavior of concrete confined by overlapping hoops at low and high strain rates," *ACI J.*, vol. 79, no. 1, pp. 13–27, 1982.

[19] I. D. Karsan and J. O. Jirsa, "Behavior of concrete under compressive loadings," *J. Struct. Devision*, vol. 95, no. ST12, pp. 2543–2563, 1969.

[20] M. Menegotto and P. E. Pinto, "Method of analysis for cyclically loaded RC plane frames including changes in geometry and non-elastic behavior of elements under combined normal," in *Proc. of IABSE symposium on Resistance and Ultimate Deformability of Structures Acted on by Well Defined Repeated Loads*, 1973, pp. 15–22.

[21] F. C. Filippou, E. P. Popov, and V. V. Bertero, "Effect of bond deterioration on hysteretic behavior of reinforced concrete joints," Berkeley, California, EERC Report UCB/EERC-83/19, 1983.